Research Repository UCD

Title	Steady-State Oscillations in Resonant Electrostatic Vibration Energy Harvesters
Authors(s)	Blokhina, Elena, Galayko, Dimitri, Basset, Philippe, Feely, Orla
Publication date	2013-04
Publication information	Blokhina, Elena, Dimitri Galayko, Philippe Basset, and Orla Feely. "Steady-State Oscillations in Resonant Electrostatic Vibration Energy Harvesters." IEEE, April 2013. https://doi.org/10.1109/TCSI.2012.2209295.
Publisher	IEEE
Item record/more information	http://hdl.handle.net/10197/3867
Publisher's statement	© 2013 IEEE. Personal use of this material is permitted. Permission from IEEE must be obtained for all other uses, in any current or future media, including reprinting/republishing this material for advertising or promotional purposes, creating new collective works, for resale or redistribution to servers or lists, or reuse of any copyrighted component of this work in other works.
Publisher's version (DOI)	10.1109/TCSI.2012.2209295

Downloaded 2026-05-01 23:37:36

The UCD community has made this article openly available. Please share how this access benefits you. Your story matters! (@ucd_oa)

© Some rights reserved. For more information

Steady-State Oscillations in Resonant Electrostatic Vibration Energy Harvesters

Elena Blokhina[1], Dimitri Galayko[2], Philippe Basset[3] and Orla Feely[1]

[1]School of Electrical, Electronic and Communications Engineering, University College Dublin, Belfield, Dublin 4, Ireland
[2]UPMC – Sorbonne Universités, 4, place Jussieu, 75005 Paris, France
[3]Université Paris-Est, ESYCOM, ESIEE Paris 2, bd Blaise Pascal - BP 99 93162 Noisy-le-Grand Cedex, France

***Abstract*—In this paper, we present a formal analysis and description of the steady-state behavior of an electrostatic vibration energy harvester operating in constant-charge mode and using different types of electromechanical transducers. The method predicts parameter values required to start oscillations, allows a study of the dynamics of the transient process, and provides a rigorous description of the system, necessary for further investigation of the related nonlinear phenomena and for the optimisation of converted power. We show how the system can be presented as a nonlinear oscillator and be analysed by the multiple scales method, a type of perturbation technique. We analyse two the most common cases of the transducer geometry and find the amplitude and the phase of steady-state oscillations as functions of parameters. The analytical predictions are shown to be in good agreement with the results obtained by behavioural modeling.**

***Index Terms*—electrostatic vibration energy harvesters, steady-state oscillations, multiple scale method, bifurcation analysis**

I. Introduction

Electrostatic (capacitive) vibration energy harvesters (e-VEHs) convert kinetic energy of the environment into electrical energy using a capacitive transducer [1]. E-VEHs are particularly suitable for microscale implementation and have become in recent years the subject of a growing area of research [2]–[11]. The main issue of e-VEH design is the optimization of converted power for given environmental conditions and given limitations of the electrical and mechanical components [12]. This optimisation requires a tool estimating the converted power for a given set of design parameters and operation conditions [13], [14]. To date, such a tool is still lacking. The architecture and operation of VEHs based on electrostatic transducers is intrinsically more complex than for the case of electromagnetic and piezoelectric VEHs [4], [15]–[17]. Because of periodic charge/discharge cycles, the system is time-variant and cannot be adequately analysed with a simple analytical approach such as linearization around an operating point. The conditioning circuit brings additional complexity to the system since its architecture and operating mode impact directly the mechanical dynamics of the resonator. For these reasons, an optimal design of an e-VEH requires a deep understanding of the overall system dynamics, including nonlinear effects.

There are practical reasons for developing a theoretical analysis. It allows the prediction and analysis of irregular and chaotic behavior for realistic configurations of the conditioning circuit as highlighted in [18]. As a result, one can bound the area of internal and external parameters of the system where stable harmonic vibrations exist. Based on that knowledge, one can predict the most effective operating parameters of the e-VEH (such as the amplitude of the mobile mass displacement) at the design stage, and thereby optimise converted power.

Indeed, most existing conditioning circuits for e-VEHs [2], [4], [5], [8] operate correctly only in the context of regular quasi-sinusoidal motion of the resonator, since their operating mode is based on the detection of the maximum and minimum of the transducer capacitance. Theoretically, in a non-regular mode there can be a large number of local maxima and minima during a particular time interval (e.g., during one period of the external vibration). In practice, the dynamics of the system over these intervals are defined by non-idealities of the conditioning circuit (for example, there is always a delay in the detection of extrema in realistic circuits) and are virtually impossible to predict. Such irregular behaviour is not compatible with an optimal operating mode of the e-VEH system, and the designer of the e-VEH must avoid such regimes. Hence, the theory should allow the analysis of irregular modes and clearly indicate the limits between regular and irregular behaviour.

The work [14] has suggested a general analytical tool for analysis of a resonant electrostatic VEH operating in the mode of strong electro-mechanical coupling. The tool proposed there introduces the amplitude-dependent mechanical impedance of the nonlinear system "conditioning circuit – capacitive transducer" that allows one to use a well-known method of analysis of electrical networks. This tool is comprehensive for those who are familiar with electronic design tools, and it provides a good agreement with behavioural modeling. However, this tool is still limited for further exploration of non-regular behaviour and does not take into account the eventual zero-frequency shift of the mobile mass position, which can be significant for transducers with asymmetric geometry (typically, a gap-closing transducer).

Building on this work, our paper presents a formal approach based on the application of the multiple scales method (MSM) to a resonant e-VEH with the most common conditioning circuit proposed in [4]. In this approach, the system is presented as a nonlinear oscillator where the electromechanical transducer generates a nonlinear force. With this conditioning circuit, the transducer operates in a constant-charge triangular QV energy conversion cycle that is considered as being the most efficient mode of operation [19]. Like the tool in [14],

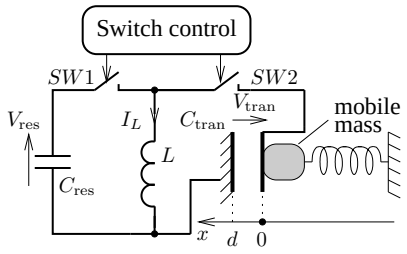

Fig. 1. Schematic view of an electrostatic vibration energy harvester.

the proposed method allows one to find parameters of steady-state oscillations (such as the amplitude and phase) as functions of parameters of the conditioning circuit, the resonator and the external acceleration. In addition, the MSM provides a straightforward route for bifurcation and stability analysis and for the analysis of transient process, and it can easily be adjusted for different types of nonlinearities such as nonlinear air damping, mechanical (spring) nonlinearity and different forms of the transducer force. In particular, the analysis presented here predicts analytically the irregular behaviour of the eVEH at weak amplitudes discovered previously by simulations in a behavioural model [18].

The validation of the analytical results is carried out by employing mixed VHDL–AMS/Eldo simulations of the e-VEH described in detail in [14]. Two VHDL–AMS/Eldo models are considered. The first one is a simplified model that implements an ideal operating regime of a capacitive transducer in constant-charge mode. The second model implements the conditioning circuit described in [4] and takes into account certain effects typical for realistic systems such as losses in diodes and finite charging times of the variable capacitors. Our analysis and simulations are carried out for two types of transducer: a gap-closing transducer whose capacitance is a hyperbolic function of the displacement and an area overlap transducer whose capacitance is a linear function of the displacement.

The paper is organised as follows. In Sec. II we discuss the architecture of the system and its governing equations. Section III describes the behavioural VHDL-AMS/Eldo models of the e-VEH. Section IV presents the MSM-based analysis of the system while and Sec. V gives the results of the application of the MSM methods to transducers with the two geometries and discusses the comparison between the simulations and analytical results.

II. Statement of the Problem

In this section, we introduce the electromechanical model used to describe our VEH devices. A simple electrostatic harvester consists of a resonator, a variable capacitor (a transducer) C_{tran} and a conditioning circuit (fig. 1). The resonator frame moves due to the external vibrations. The displacement x of the mobile mass with respect to the frame is also affected by the transducer force f_t. Therefore, the equation defining x is

$$\ddot{x} + (b/m)\dot{x} + \omega_0^2 x = A_{ext}\cos(\omega_{ext}t + \vartheta_0) + f_t/m \qquad (1)$$

where m is the mass of the resonator, b is the damping factor, $\omega_0 = \sqrt{k/m}$ is the natural frequency, k is the spring constant, A_{ext} is the acceleration amplitude of external vibrations, ω_{ext} is the external frequency and ϑ_0 is the initial phase of the external vibrations.

The transducer force f_t depends on the transducer voltage V_{tran} and on the mobile mass position x:

$$f_t(x, V_{tran}) = \frac{V_{tran}^2}{2}\frac{dC_{tran}}{dx} \qquad (2)$$

where V_{tran} is generated by the conditioning circuit from fig. 1 proposed in [4] that implements the constant-charge triangular QV energy conversion cycle. The conditioning circuit discharges the transducer to zero when the transducer capacitance is at a local minimum and charges it to a charge Q_0 when its capacitance is at a local maximum. The energy conversion is achieved when the transducer capacitance decreases keeping its charge constant (Q_0). During this process, mechanical energy is converted into electrical energy, and the transducer acts as a damper in the mechanical domain. In the case of transducers with monotonously increasing $C_{tran}(x)$ characteristics, the voltage generated by the transducer depends on the sign of the mobile mass velocity: $V_{tran} = 0$ if $\dot{x} > 0$ and $V_{tran} = Q_0 C_{tran}(x(t))$ if $\dot{x} < 0$. Hence, the force is a piecewise defined function : $f_t = 0$ if $\dot{x} > 0$ and $f_t = f_t(x, Q_0/C_{tran}(x))$ otherwise, and will be referred later as $f_t(x, \dot{x})$.

At a *local maximum* of C_{tran}, the conditioning circuit fixes three electrical quantities on the transducer: the charge Q_0, the voltage V_0 and the energy W_0. Only one of the three can be fixed independently from the others since they are related by the following expressions:

$$Q_0 = C_{max}V_0\,, \qquad W_0 = \frac{1}{2}\frac{Q_0^2}{C_{max}} \qquad (3)$$

Here C_{max} is the local maximum value of the C_{tran}. It is important to understand that C_{max} is a dynamic quantity which may change at each local maximum of C_{tran} and which is constant during the time intervals between two consecutive local maxima. C_{max} is constant in a steady-state harmonic mode.

At a *local minimum* the three quantities are set to zero. The quantity (one from the three) that is independently fixed to a non-zero value at a local maximum depends on the architecture of the conditioning circuit. In this paper, we consider the most common case valid for the circuit in fig. 1 where the energy W_0 is fixed [4] (see the description of the behavioral model in Sec. III).

Whatever quantity is fixed on the transducer at a local maximum of C_{tran}, the charge Q_0 does not change until the next local minimum of C_{tran} is reached. The electromechanical energy conversion is carried out during the time interval corresponding to the motion of the mobile plate from C_{max} to C_{min} positions. This energy conversion mode is called in literature the *constant-charge operating mode* of the transducer, which underlines the fact the transducer keeps a constant electrical charge during the electrical energy generation.

For an area overlap transducer [20], the capacitance is $C_{tran} = C_0 + \alpha_{tran}x$ and $V_{tran} = Q_0/C_{tran} =$

$\sqrt{2W_0C_{max}}/C_{tran}$. The expression for the transducer force in this case is

$$f_{t,1}(x,\dot{x}) = \begin{cases} \frac{W_0\alpha_{tran}(1+\alpha_{tran}x_{max}/C_0)}{C_0(1+\alpha_{tran}x/C_0)^2}, & v \le 0 \\ 0 & v > 0 \end{cases} \quad (4)$$

Here x_{max} is the local maximum of x, defined similarly to C_{max}.

In order to reduce the number of parameters and outline only essential ones, the following normalised variables are introduced: time $\tau = \omega_0 t$, dissipation $\beta = b/(2m\omega_0)$, normalised external vibration frequency $\Omega = \omega_{ext}/\omega_0$, $y = \alpha_{tran}x/C_0$, $\alpha = \alpha_{tran}A_{ext}/(C_0\omega_0^2)$ and $\kappa_0 = \alpha_{tran}^2 W_0/(C_0^2 m\omega_0^2)$. Equation (1) is now written as

$$y'' + 2\beta y' + y = f_t(y,y') + \alpha\cos(\Omega\tau + \theta_0) \quad (5)$$

where the prime denotes the derivative with respect to dimensionless time τ and the function $f_t(y,y')$ is the normalised version of (4):

$$f_{t,1}(y,y') = \begin{cases} \frac{\kappa_0(1+y_{max})}{(1+y)^2}, & y' \le 0 \\ 0 & y' > 0 \end{cases} \quad (6)$$

The same equation (5) may be used to describe the system with other types of transducers. For the transducer with hyperbolic capacitance function [14], [18] $C_{tran}(x) = C_0/(1-x/d)$, the transducer force is

$$f_{t,2}(x,v) = \begin{cases} \frac{W_0}{d(1-x_{max}/d)}, & v \le 0 \\ 0 & v > 0 \end{cases} \quad (7)$$

Here d is the transducer gap at rest ($f_{tran} = 0$ and $A_{ext} = 0$) and x_{max} is the maximum value of displacement x. Introducing the variables and parameters $y = x/d$, $\alpha = A_{ext}/(d\omega_0^2)$ and $\nu_0 = W_0/(d^2 m\omega_0^2)$, one obtains the force in the form

$$f_{t,2}(y,y') = \begin{cases} \frac{\nu_0}{(1-y_{max})}, & y' \le 0 \\ 0 & y' > 0 \end{cases} \quad (8)$$

In this study, we consider the geometry of the transducers and resonator as fixed (the mass, the natural frequency and the transducer dimensions are constant), whereas the external acceleration amplitude A_{ext} and the energy W_0 are the design parameters which may vary and affect the behaviour of the system. By consequence, for the normalised equation, there are two control parameters of the dynamical system: α and κ_0 for area overlap transducer and α and ν_0 for gap-closing transducer.

Numerical examples will be presented with typical parameters of systems (4) and (7), as given in Table I. The values are taken from [14] and [16].

TABLE I
PARAMETERS OF THE SYSTEMS

	Area overlap	hyperbolic
m	$50 \cdot 10^{-6}$ kg	$200 \cdot 10^{-6}$ kg
b	$2.16 \cdot 10^{-3}$ Nsm^{-1}	$\sqrt{2} \cdot 10^{-3}$ Nsm^{-1}
k	150 Nm^{-1}	300 Nm^{-1}
d	—	$20 \cdot 10^{-6}$ m
S	—	$10 \cdot 10^{-4}$ m^2
α_{tran}	10^{-6} Fm^{-1}	—
C_0	$150 \cdot 10^{-12}$ F	—
L	$3 \cdot 10^{-3}$ H	—
W_0	$< 10 \cdot 10^{-8}$ J	$< 3 \cdot 10^{-8}$ J
A_{ext}	< 30 ms^{-2}	< 10 ms^{-2}

III. Behavioural Modeling of the E-VEH

The modeling of the e-VEH has been carried out employing a mixed SPICE and behavioural description implemented in the VHDL-AMS/Eldo environment provided with the AdvanceMS tool of Mentor Graphics. The conditioning circuit is implemented as an electrical network described by an Eldo netlist (Eldo is a commercial variant of the SPICE simulator). The transducer and resonator are described by a VHDL-AMS model. We consider two models that have different implementations of the condition circuit from fig. 1. The first model employs an ideal simple circuit and the second model employs a circuit that includes certain 'nonidealities' that can be found in realistic circuits.

A. VHDL-AMS Model of the Transducer/Resonator

The VHDL-AMS language is a powerful tool that allows one to describe physical systems defined by lumped-parameter differential equations. This language is particularly suitable for the description of behaviour of systems interfaced with electrical networks [21]. A VHDL-AMS model of the transducer/resonator block can be seen as an electrical dipole behaving as a variable capacitor. The capacitance variation is obtained through resolution of Newtonian equations written for the resonator which also takes into account the force f_t generated by the transducer. Presented in [18], the VHDL-AMS model of the transducer/resonator block is a system of physical differential equations:

$$\begin{aligned} & f_t = \frac{1}{2}V_{tran}^2\frac{\partial C_{tran}}{\partial x}, \quad C_{tran} = C_{tran}(x), \\ & -kx - \mu\dot{x} + f_t = m\ddot{x} - ma_{ext}(t), \\ & i = \dot{q}, \\ & q = C_{tran}V_{tran} \end{aligned} \quad (9)$$

Here $a_{ext}(t)$ is the known acceleration of the external vibrations, q, i and v are the charge, current and voltage through the terminals of the variable transducer capacitor. The model solves these five equations for five unknown quantities: f_t, x, q, C_{tran} and i or v. One of the two latter quantities or a relation between them is defined by the electrical network connected to the modeled dipole.

B. Mixed VHDL-AMS/Eldo Model of the Conditioning Circuit

In order to formally validate the theory presented in the paper, we used the conditioning circuit model shown in fig. 2. Its goal is to create an electrical context for the transducer that exactly corresponds to the constant-charge energy conversion regime described by the equations given in Section II [4]. The switches $SW1$ and $SW2$ are driven by short pulses corresponding to the moments of local maxima and minima of C_{tran}. These pulses are long enough to charge the transducer

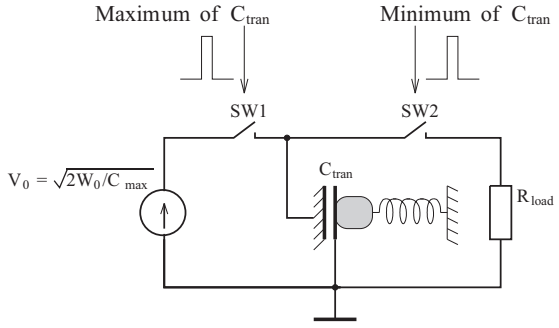

Fig. 2. Simplified idealised conditioning circuit.

at a local maximum of C_{tran} to V_0 and to discharge it through a small load resistance when C_{tran} reaches a local minimum. The voltage V_0 is defined as a function of the value of the local maximum of C_{tran} through the formula $W_0 = V_0^2 C_{max}/2$, where W_0 is a constant parameter of the model. This model emulates the ideal electrical environment for a transducer operating in constant-charge mode and requires few resources for simulations. It is not realistic and is only used for the intermediate theory validation.

A more realistic model of the conditioning circuit is given in fig. 3. It is directly based on the circuit presented in [4]. Initially, the large reservoir capacitor C_{res} is charged up to some voltage V_{res} that is assumed to be constant since C_{res} is large. The model is provided with blocks described in VHDL-AMS allowing the detection of a local maximum and minimum of C_{tran} and of a local maximum of the inductor current I_L.

When a local maximum of C_{res} is detected, the switch $SW1$ is closed for a fixed time τ, thus loading the inductor to a current

$$I_L = \frac{\tau V_{res}}{L} \tag{10}$$

The corresponding energy of the inductor is

$$W_0 = L I_L^2/2 \tag{11}$$

After the time τ, $SW1$ is open and the inductor current flows through the diode $D2$ and charges C_{tran} (forward charge transfer). Note that whatever the value of C_{tran} is at that moment, the inductor gives it the energy W_0 that is a free design parameter of this architecture and is uniquely related with L, V_{res} and τ.

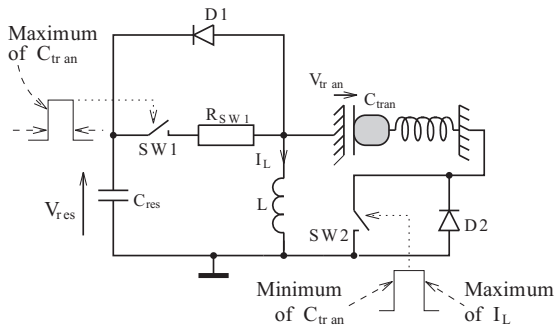

Fig. 3. Model of the realistic conditioning circuit [4].

TABLE II
PARAMETERS OF VHDL-AMS/ELDO MODELS

Parameter name	Value
C_{res}	10 μF
R_{SW1}, R_{load}	0.001 Ω
W_0 for the gap-closing transducer: for the area overlap transducer:	 15...25 nJ 10...100 nJ
L	10 mH
V_{res}	3V
Max/min detector on C_{max} sampling frequency:	 1 MHz
Max/min detector on C_{max} sampling frequency:	 100 MHz
Transducer-resonator parameters	As in table I

Both processes (the inductor and capacitor charging) are very fast and they take place during a time that is negligible with respect to the variation period of C_{tran}. This is ensured by the appropriate choice of the value of the inductance L.

After that, both switches are closed, and the electrostatic transducer operates in constant-charge mode. When C_{tran} reaches a local minimum, the switch $SW2$ is opened, allowing the transducer to discharge through the inductor. When the voltage on C_{tran} is zero (the current in the inductor is maximal), the transducer is disconnected from the inductor by the switch $SW2$. The energy accumulated in the inductor is transferred to C_{res} through the diode $D1$.

Table II presents the numerical parameters of the circuit operation and the timing of the switch operation. The maximum/minimum detectors regularly sample the input quantity and search for a local maximum/minimum by analysing the last three sampled points (in practice, the maximum detection is done by analog signal processing [4]). Note that the characteristic time of the electromechanical energy conversion defined by the rate of the mobile mass motion is much larger than the time required for the energy transfer between C_{res} and C_{tran}. Hence, the detector detecting an I_L maximum operates at much higher frequency than the C_{tran} max/min detector.

The advantage of this model for our study is that its architecture is very close to the realistic circuit and it accounts for realistic parasitic effects such as losses in the flyback diodes. However, the presented model has two minor drawbacks for the theory validation. Firstly, it does not correspond exactly to the mathematical model described in Sec. II since it includes the diodes and considers a small finite time for the charging/discharging processes, and its dynamics may be slightly different from those described by the mathematical model. Secondly, the simulation time is long. These are the reasons why the idealised circuit of fig. 2 is introduced as an intermediate validation step.

IV. MULTIPLE SCALES METHOD

The method of multiple scales (MSM) is an asymptotic method that is often applied for the analysis of weakly nonlinear oscillators [22], both autonomous and under external excitation. The idea behind this method is to present oscillations in a quasi-harmonic form and to find adjustments to oscillation characteristics, such as amplitude and phase,

that result from the nonlinearity. The methods is known to be an effective tool for a range of system, from classical the Duffing's oscillator [22] to voltage controlled oscillators [23] and recently was employed to study nonlinear vibrations of piezoelectric harvesters [24]. In this section, the application of the MSM to the e-VEH system is presented. More details about the standard implementation of the method can be found in [22].

A. Standard Implementation of the Method

In eq. (5), the dimensionless parameters β, κ_0, ν_0 and α are relatively small with respect to unity. Since we consider a resonant harvester, we also introduce a small σ representing the external vibration frequency mismatch with the natural resonance frequency of the resonator: $\Omega = 1+\sigma$. To emphasise the terms with small parameters, we introduce a small quantity ε and replace them by the following products: $\beta = \varepsilon\tilde{\beta}$, $\alpha = \varepsilon\tilde{\alpha}$, and $\sigma = \varepsilon\tilde{\sigma}$. We also note the functions f_t are the product of the coefficients κ_0 and ν_0 and dimensionless ratios containing y or y_{max}, so we can also present $\kappa_0 = \varepsilon\tilde{\kappa}_0$ and $\nu_0 = \varepsilon\tilde{\nu}_0$. In order to put them into the correct order of the small parameter ε in the method, we will note $f_t = \varepsilon\tilde{f}_t$. Thus,

$$y'' + 2\varepsilon\tilde{\beta}y' + y = \varepsilon\tilde{f}_t(y, y') + \varepsilon\tilde{\alpha}\cos(\tau + \varepsilon\tilde{\sigma}\tau + \theta_0) \quad (12)$$

The multiple scales method is a perturbation method that introduces the time scales $T_k = \varepsilon^k\tau$. In this case, the system dynamics defined by the process $y(\tau)$ is now dependent on different time scales. The time derivatives are now given by

$$\frac{d}{d\tau} = D_0 + \varepsilon D_1, \quad \frac{d^2}{d\tau^2} = D_0^2 + 2\varepsilon D_0 D_1 \quad (13)$$

where $D_k = \partial/\partial T_k$, $k = 0, 1, \ldots$. For displacement y, a standard expansion for perturbation method is used:

$$y = y_0(T_0, T_1) + \varepsilon y_1(T_0, T_1), \quad (14)$$

Equation (12) now can be rewritten as follows

$$\begin{aligned}&(D_0^2 + 2\varepsilon D_0 D_1)(y_0 + \varepsilon y_1) + 2\varepsilon\tilde{\beta}(D_0 + \varepsilon D_1)\times\\ &\times (y_0 + \varepsilon y_1) + y_0 + \varepsilon y_1 = \varepsilon\tilde{f}_t\,[y_0 + \varepsilon y_1,\\ &(D_0 + \varepsilon D_1)(y_0 + \varepsilon y_1)] + \varepsilon\tilde{\alpha}\cos(T_0 + \tilde{\sigma}T_1 + \theta_0)\end{aligned} \quad (15)$$

Collecting orders 0 and 1 of the parameter ε, and neglecting order 2 and higher, we obtain two equations:

$$D_0^2 y_0 + y_0 = 0\,, \quad (16a)$$

$$\begin{aligned}&D_0^2 y_1 + y_1 = -2D_0 D_1 y_0 - 2\tilde{\beta}D_0 y_0 +\\ &\tilde{f}_t(y_0, D_0 y_0) + \tilde{\alpha}\cos(T_0 + \tilde{\sigma}T_1 + \theta_0)\end{aligned} \quad (16b)$$

In (15) the terms with ε in the arguments of $\tilde{f}_t$ give second-order terms in the expansion of f_t over the powers of ε, hence we neglect them in (16b). The solution of (16a) is

$$y_0 = A(T_1)e^{iT_0} + c.c. = a(T_1)\cos(\tau + \varphi(T_1)) \quad (17)$$

where the slow complex amplitude $A = (a/2)\exp(i\varphi)$ is expressed through the real slow amplitude a, and $c.c.$ stands for the complex conjugate. In expression (16b), the function $\tilde{f}_t(y_0, D_0 y_0)$ is a periodic function of T_0 with period 2π (as well as y_0) and, therefore, we can use the Fourier series for the force $\tilde{f}_t$. Recalling that the system is high-Q resonant, we limit the series to the first harmonic:

$$\begin{aligned}&\tilde{f}_t(y_0, D_0 y_0) = \tilde{f}_0(a) +\\ &+ \tilde{a}_1(a)\cos(T_0 + \varphi) + \tilde{b}_1(a)\cos(T_0 + \varphi)\end{aligned} \quad (18)$$

where $\tilde{f}_0$, $\tilde{a}_1$ and $\tilde{b}_1$ are the following coefficients of the Fourier series

$$\begin{aligned}\tilde{f}_0(a) &= \frac{1}{2\pi}\int_0^{2\pi}\tilde{f}_t(a\cos\theta, -a\sin\theta)d\theta\\ \tilde{a}_1(a) &= \frac{1}{\pi}\int_0^{2\pi}\tilde{f}_t(a\cos\theta, -a\sin\theta)\cos(\theta)d\theta\\ \tilde{b}_1(a) &= \frac{1}{\pi}\int_0^{2\pi}\tilde{f}_t(a\cos\theta, -a\sin\theta)\sin(\theta)d\theta\end{aligned} \quad (19)$$

Equivalently, in the complex representation

$$\tilde{f}_t(y_0, D_0 y_0) = \tilde{f}_0(a) + [\tilde{c}_1(a)e^{iT_0 + i\varphi} + c.c.] \quad (20)$$

where complex $\tilde{c}_1$ is expressed through real $\tilde{a}_1$ and $\tilde{b}_1$

$$\tilde{c}_1(a) = (\tilde{a}_1(a) - i\tilde{b}_1(a))/2 \quad (21)$$

After the solution for y_0 is substituted into (16b), we collect the terms that contain $\exp(iT_0)$ since they lead to linear resonance of the undamped system. Equation (16b) yields one equation to find y_1 and one equation for complex $A(T_1)$:

$$D_0^2 y_1 + y_1 = \tilde{f}_0\,, \quad (22a)$$

$$\begin{aligned}&-2i\dot{A}e^{iT_0} - 2\tilde{\beta}iAe^{iT_0} + \tilde{c}_1(a)e^{iT_0 + i\varphi} +\\ &+ \tilde{\alpha}/2e^{i(T_0 + \tilde{\sigma}T_1 + \theta_0)} + c.c. = 0\end{aligned} \quad (22b)$$

From expression (22a), it follows that $y_1 = \tilde{f}_0$ and, as a consequence, εy_1 represents the average (zero frequency) shift of the mobile mass displacement due to the transducer force. Let us denote for convenience:

$$y_{av} = \varepsilon y_1 = \varepsilon\tilde{f}_0. \quad (23)$$

Therefore, the total solution will take the form

$$y(\tau) = y_0 + \varepsilon y_1 = y_{av} + a\cos(\tau + \varphi) \quad (24)$$

Dividing (22b) into real and imaginary parts, one obtains equations for the slow amplitude a and the phase $\psi = \tilde{\sigma}T_1 + \theta_0 - \varphi$:

$$\begin{aligned}\dot{a} &= -\tilde{\beta}a - \frac{\tilde{b}_1(a)}{2} + \frac{\tilde{\alpha}}{2}\sin\psi,\\ a\dot{\psi} &= a\tilde{\sigma} + \frac{\tilde{a}_1(a)}{2} + \frac{\tilde{\alpha}}{2}\cos\psi\end{aligned} \quad (25)$$

It is relevant to note that this system of differential equations provides information about transient dynamics of the system, and allows one to explore the dynamics around multiple stable points and identify different possible stable modes.

Let us find the steady-state solution a_0 and ψ_0 from the condition $\dot{a} = 0$ and $\dot{\psi} = 0$. For the phase ψ_0 one obtains a

set of equations

$$\begin{aligned}\frac{\tilde{\alpha}}{2}\sin\psi_0 &= \tilde{\beta}a_0 + \frac{\tilde{b}_1(a_0)}{2},\\ \frac{\tilde{\alpha}}{2}\cos\psi_0 &= -a_0\tilde{\sigma} - \frac{\tilde{a}_1(a_0)}{2}\end{aligned} \tag{26}$$

The equation for the amplitude a_0 can now be found from (26)

$$\frac{\tilde{\alpha}^2}{4} = \left(\tilde{\beta}a_0 + \frac{\tilde{b}_1(a_0)}{2}\right)^2 + \left(a_0\tilde{\sigma} + \frac{\tilde{a}_1(a_0)}{2}\right)^2 \tag{27}$$

Expressions (24), (26) and (27) define the steady-state response of the nonlinear oscillator (5) to the external driving and the nonlinear force f_t. Note that by multiplying both sides of (27) by ε^2 we can rewrite this equation with the original values of α, β and σ in the same form.

The steady-state solution therefore is

$$y(\tau) = y_{av,0} + a_0\cos((1+\sigma)\tau + \theta_0 - \psi) \tag{28}$$

where we have used the index '0' to emphasize that y_{av}, a and ψ are steady-state characteristics.

B. Stability of Steady-State Solutions

Formally, $\mathbf{x}_0 = (a_0, \psi_0)$ is a fixed point of the set (25). To analyse its stability, we introduce small perturbations $a_1(T_1)$ and $\psi_1(T_1)$ to a_0 and ψ_0 and substitute $a(T_1) = a_0 + a_1$ and $\psi(T_1) = \psi_0 + \psi_1$ into (25). The linearised system describing the evolution of $\mathbf{x}_1 = (a_1, \psi_1)$ has the following form

$$\begin{pmatrix}\dot{a}_1\\ \dot{\psi}_1\end{pmatrix} = \begin{pmatrix}-\tilde{\beta} - \frac{\tilde{b}_1'}{2} & \frac{\tilde{\alpha}}{2}\cos\psi_0\\ \frac{1}{a_0}\left(\tilde{\sigma} + \frac{\tilde{a}_1'}{2}\right) & -\frac{\tilde{\alpha}}{2a_0}\sin\psi_0\end{pmatrix}\begin{pmatrix}a_1\\ \psi_1\end{pmatrix} \tag{29}$$

where the matrix is in fact the Jacobian $J(\mathbf{x})$ obtained from (25) and taken at $\mathbf{x} = \mathbf{x}_0$.

Thus, stability of the fixed point $\mathbf{x}_0 = (a_0, \psi_0)$ is defined by the eigenvalues of the matrix in (29). According to the Routh-Hurwitz criterion, the point (a_0, ψ_0) is stable if the following conditions are fulfilled:

$$\begin{aligned}&2\tilde{\beta} + \frac{\tilde{b}_1'}{2} + \frac{\tilde{b}_1}{2a_0} > 0\\ &\left(\tilde{\beta} + \frac{\tilde{b}_1'}{2}\right)\left(\tilde{\beta} + \frac{\tilde{b}_1}{2a_0}\right) + \left(\tilde{\sigma} + \frac{\tilde{a}_1'}{2}\right)\left(\tilde{\sigma} + \frac{\tilde{a}_1}{2a_0}\right) > 0\end{aligned} \tag{30}$$

If the above conditions are not fulfilled, the orbit that is defined by these a_0 and ψ_0 is unstable (a saddle orbit). The above stability condition is necessary, but not sufficient. We note here that for nonlinear oscillators, it is very typical that the increase of the external force amplitude or other parameters leads to bifurcations of previously stable orbits and eventually, to irregular, chaotic behaviour. Though these dynamics are beyond the scope of this paper, the results obtained by the MSM can be used in a further analysis. We report the results of this research in [25].

C. Improving Accuracy for the Estimation of the Zeroth Harmonic

The described above algorithm works very well if the average shift $y_{av,0} = \varepsilon y_1$ is relatively small compared to the amplitude a_0 of oscillations (see the discussion on the comparison between the model simulations and the theory in the next section). However, for the gap-closing transducer whose force is expressed by (8) the constant shift of oscillations can be large and even larger than a_0 [18]. This leads to a non-negligible error in y_{av} provided by the standard implementation of the MSM that we described in Sec. IV*A*. This error appears from the underestimation of the force $\tilde{f}_t$ that can be relatively large and that produces the average shift of $y(\tau)$.

In order to accurately incorporate this effect into the model, we can use the solution (24) when presenting $\tilde{f}_t$ as a Fourier expansion. Since the transducer forces (8) depend on the maximum displacement that we define as $y_{max} = y_{av} + a$, the Fourier coefficients will be the functions of both, y_{av} and a: $\tilde{f}_0(y_{av}, a)$, $\tilde{a}_1(y_{av}, a)$ and $\tilde{b}_1(y_{av}, a)$. Practically, it means that the Fourier expansion is carried out for $\tilde{f}_t(y_0 + \varepsilon y_1)$ in (16b). Equations (26) and (27) are rewritten as

$$\begin{aligned}\frac{\tilde{\alpha}}{2}\sin\psi_0 &= \tilde{\beta}a_0 + \frac{\tilde{b}_1(y_{av,0}, a_0)}{2},\\ \frac{\tilde{\alpha}}{2}\cos\psi_0 &= -a_0\tilde{\sigma} - \frac{\tilde{a}_1(y_{av,0}, a_0)}{2}\end{aligned} \tag{31}$$

and

$$\frac{\tilde{\alpha}^2}{4} = \left(\tilde{\beta}a_0 + \frac{\tilde{b}_1(y_{av,0}, a_0)}{2}\right)^2 + \left(a_0\tilde{\sigma} + \frac{\tilde{a}_1(y_{av,0}, a_0)}{2}\right)^2 \tag{32}$$

These equations have three unknown variables: $y_{av,0}$, a_0 and ψ_0. One more equation is required to obtain a self-consistent system and it is obtained from equation (23) for the average shift $y_{av,0}$, where we assume that $\tilde{f}_0$ depends on a_0 and on $y_{av,0}$ itself:

$$y_{av,0} = \tilde{f}_0(y_{av,0}, a_0) \tag{33}$$

Solving the four expressions given by (31), (32) and (33), we find a_0 and $y_{av,0}$ and ψ_0 to be used in solution (28).

Finally, we briefly note how we derived a criterion similar to (30) to obtain the necessary condition for stability. There are three actual variables in the system: the amplitude a, the phase ψ and the shift y_{av}. The evolution of a and ψ is given by (25) with the difference that now $\tilde{a}_1$ and $\tilde{b}_1$ are functions of a and y_{av}. The third equation that determines the evolution of y_{av} is obtained by differentiating expression (33). Therefore, the dynamics of the variable are given by the equations

$$\begin{aligned}\dot{a} &= -\tilde{\beta}a - \frac{\tilde{b}_1(y_{av}, a)}{2} + \frac{\tilde{\alpha}}{2}\sin\psi = F(a, \psi, y_{av}),\\ \dot{\psi} &= \tilde{\sigma} + \frac{\tilde{a}_1(y_{av}, a)}{2a} + \frac{\tilde{\alpha}}{2a}\cos\psi = G(a, \psi, y_{av}),\\ \dot{y}_{av} &= \frac{1}{1 - \partial\tilde{f}_0/\partial y_{av}}\frac{\partial\tilde{f}_0}{\partial a}\dot{a} = H(a, \psi, y_{av})\end{aligned} \tag{34}$$

Now $\mathbf{x}_0 = (a_0, \psi_0, y_{av,0})$ is a fixed point of (34). Similarly to Sec. IV*B*, the small perturbations $\mathbf{x}_1 = (a_1, \psi_1, y_{av,1})$ from $\mathbf{x}_0$ are introduced into (34). The dynamics of the perturbations are defined by the equation

$$\dot{\mathbf{x}}_1^T = J(\mathbf{x})|_{\mathbf{x}=\mathbf{x}_0}\,\mathbf{x}_1^T \tag{35}$$

where the Jacobian $J(\mathbf{x})$ is obtained from (34) and taken at $\mathbf{x}_0 = (a_0, \psi_0, y_{av,0})$. In this case we obtain a cubic polynomial

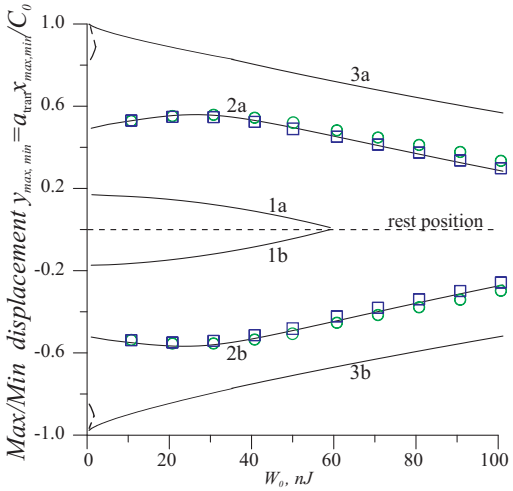

Fig. 4. Area overlap transducer: the envelope (maximum and minimum values) of oscillations as a function of the energy W_0 at $A_{ext} = 5\ m/s^2$ (line 1), $A_{ext} = 15\ m/s^2$ (line 2) and $A_{ext} = 25\ m/s^2$ (line 3). Marks 'a' and 'b' denote the maximum and minimum values of the displacement respectively. The zero displacement or the rest position is shown by the dashed line. Squares show the envelope obtained from VHDL-AMS simulations of the idealised model from fig. 2 while circles show the simulations of the realistic model from fig. 3.

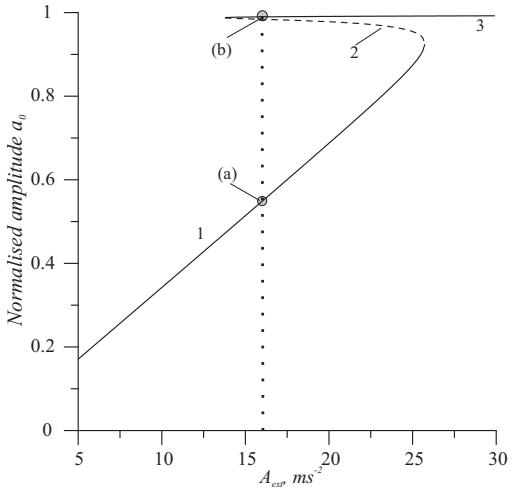

Fig. 5. Area overlap transducer: bifurcation diagram versus A_{ext} (at the fixed energy $W_0 = 375pJ$) showing to branches that correspond to stable orbits (solid lines) and a branch that correspond to an unstable orbit (dashed line). Over a range of the bifurcation parameter A_{ext}, the two stable orbits coexist. Particular examples of oscillations that correspond to the two stable branches at $A_{ext} = 16\ m/s^2$ marked (a) and (b) are shown in fig. 7.

to find the eigenvalues of J and we state the same necessary condition: in order for a solution to be stable, all real parts of the eigevalues must be negative.

V. Steady-State Oscillations: Particular Examples of the Transducer

A. Steady-State Oscillations

Let us investigate the two particular cases of the transducer. For the area overlap transducer with f_t defined as (6), the coefficients of the Fourier series are

$$f_0(a) = \frac{\kappa_0}{2(1-a)\sqrt{1-a^2}}$$
$$a_1(a) = -\frac{\kappa_0 a}{(1-a)(1-a^2)^{1/2}}, \quad b_1(a) = \frac{2\kappa_0}{\pi(1-a)} \tag{36}$$

and they are substituted into (26) and (27). The envelope of oscillations (i.e the maximum $y_{max} = y_{av,0} + a_0$ and the minimum $y_{min} = y_{av,0} - a_0$ values of the oscillation) as a function of the energy W_0 is shown in fig. 4 at three different values of the external acceleration A_{ext}. Note a slight asymmetry of the envelope: there is a non-zero average shift of oscillations that becomes more pronounced at $W_0 > 50\ nJ$.

At large accelerations A_{ext} and small energies W_0 when the oscillations of the resonator are large the system is multistable: there are three coexisting solutions of (27) with one of them unstable according to the criterion (30). Such an unstable solution can never be observed in numerical simulations of the original system (5) or in a realistic device. Alternatively, we can fix W_0 and vary A_{ext}, to see a bifurcation diagram of the parameter A_{ext} in detail (fig. 5). The two solutions, marked by 1 and 3 in fig. 5, are stable orbits that one can observe in numerical simulations by setting different initial conditions as is shown, while curve 2 shows the unstable branch.

In the case of the gap-closing transducer, the coefficients of the first Fourier harmonics are

$$f_0(y_{av}, a) = \frac{\nu_0}{2(1-y_{av}-a)}, \quad a_1(y_{av}, a) = 0,$$
$$b_1(y_{av}, a) = \frac{2\nu_0}{\pi(1-y_{av}-a)} \tag{37}$$

and they are substituted into (31), (32) and (33) in order to obtain a more accurate solution. The envelope of oscillations as a function of the energy W_0 for the gap-closing transducer is shown in fig. 6 at different values of the external acceleration

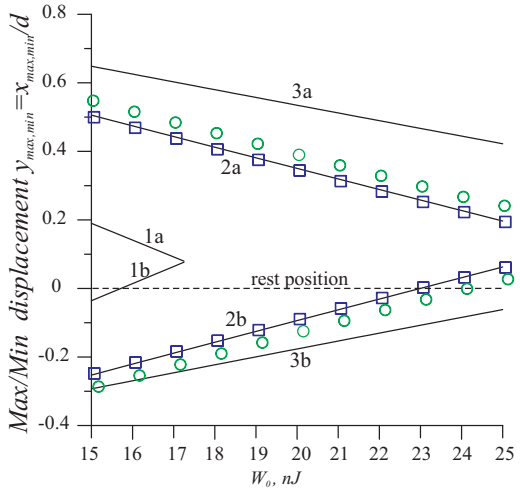

Fig. 6. Gap-closing transducer: the envelope (maximum and minimum values) of oscillations as a function of W_0 at $A_{ext} = 3\ m/s^2$ (line 1), $A_{ext} = 5\ m/s^2$ (line 2) and $A_{ext} = 7\ m/s^2$ (line 3). Marks 'a' and 'b' denote the maximum and minimum values of the displacement respectively. The zero displacement or the rest position is shown by the dashed line. Squares show the envelope obtained from VHDL-AMS simulations of the idealised model from fig. 2 while circles show the simulations of the realistic model from fig. 3.

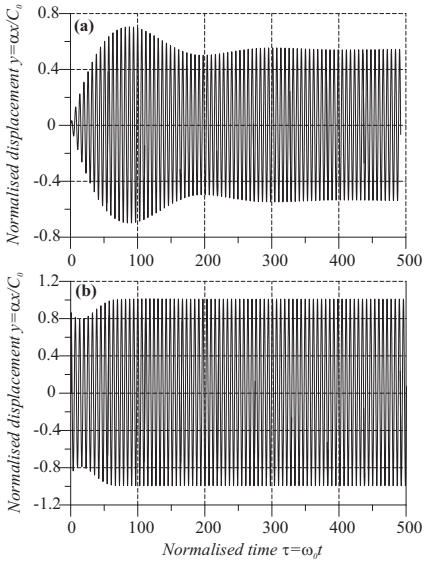

Fig. 7. Area overlap transducer: coexisting oscillations at $W_0 = 375pJ$ and $A_{ext} = 16\ m/s^2$. Two waveforms corresponds to the lower and upper branches at the points marked as (a) and (b) in fig. 5.

A_{ext}. In this case the asymmetry of the envelope is stronger: there are such energies W_0 that both, maximum $y_{av,0} + a_0$ and minimum $y_{av,0} - a_0$, are above the rest (zero) position.

Note that in this case, there also exist multiple solutions for a_0 and ψ_0 at certain W_0 and A_{ext}, i.e. formally this system is also multistable. However, the other roots of (27) are greater than unity and, as follows from the expressions (8), they lie in the "unphysical" region for this system. The only physical solution is stable according to the criterion described in IV*C*.

B. Comparison with VHDL–AMS/Eldo modelling

Numerical simulation was carried out with the VHDL–AMS/Eldo models described in Sec. III. Firstly, we compare the simulations with the analytically calculated envelope of oscillations in fig. 4 and fig. 6 for the two transducers. The results of the VHDL–AMS/Eldo simulations shown by squares for the idealised model (from fig. 2) and by circles for the realistic model (from fig. 3). While the idealised model agrees very well with the theory for the both transducers, there is a slight discrepancy with the realistic model. We recall that the realistic model includes certain parasitic effects such as losses on the diodes. Therefore, the realistic circuit does not extract mechanical energy from the resonator as effectively as the idealised circuit. This causes the amplitude of vibrations in the resonator to be slightly larger than it could be in the ideal system.

Fig. 7 presents the simulation results for the normalised displacement $y(\tau)$ obtained with different initial conditions $y(0)$ and $y'(0)$. Numerical simulations agree with the predictions of the MSM: the amplitude of the waveform 7(a) corresponds to the point (a) on the lower branch of the bifurcation diagram 5 while the amplitude in fig. 7(b) corresponds to the upper branch of that diagram and is marked as (b). We note that in this case the observed dynamics are somewhat similar to those of the Duffing oscillator under a harmonic excitation.

C. Necessary Conditions to Start Oscillations

From figs. 4 and 6, it is clearly seen that there exist values of the circuit control parameters W_0 and the acceleration A_{ext} for which there are no positive values of steady-state amplitude a_0 (see, for example, how the lines marked by 1 cross the horizontal axis in figs. 4 and 6). Since a_0 denotes the amplitude of oscillations, it has a physical meaning if it is positive. We can summarise this as follows. At a given W_0 there exists A_{ext}^{min} such that the system oscillates if $A_{ext} > A_{ext}^{min}$. And vice versa, at a given A_{ext} there exist W_0^{max} such that the system oscillates if $W_0 < W_0^{max}$. The existence of a minimal A_{ext} was discovered in a behavioral model in [18]. If this condition on W_0 and A_{ext} is not fulfilled, the operating mode of the e-VEH is irregular and uncontrollable in a realistic context.

Firstly we give a detailed example for the area overlap transducer (6) since the expression for A_{ext}^{min} and W_0^{max} can be obtained for it in a very simple form. Let us assume that $a_0 = 0$ in (27). This condition will provide us with a *necessary condition* to start oscillations. For the dimensionless parameters one obtains a simple expression

$$\alpha^2 = a_1^2(a_0)\big|_{a_0=0} + b_1^2(a_0)\big|_{a_0=0} \tag{38}$$

Substituting (36) into (38), one finds the relations between the normalised acceleration α^{min} (or A_{ext}^{min}) and given normalised circuit parameters κ_0 (or W_0) :

$$\alpha^{min} = 2\kappa_0/\pi, \qquad A_{ext}^{min} = \frac{2\alpha_{tran}W_0}{\pi m C_0} \tag{39}$$

The inverse expressions that relate the boundary values of the circuit control parameter W_0^{max} with some given external acceleration A_{ext} are easily obtained from the above. Let us give a numerical example: what maximal value of W_0 should be fixed on the transducer to obtain oscillations at $A_{ext} = 5\ m/s^2$? From (39) it follows that $W_0^{max} = 59\ nJ$. This corresponds exactly to the point in fig. 4 where the envelope disappears (this A_{ext} corresponds to the lines 1a and 1b). Therefore, no oscillations are possible if $W_0 > W_0^{max}$.

For the gap-closing transducer one solves the set of equations (32) and (33):

$$\begin{aligned} &\alpha^2 = a_1^2(y_{av,0}, a_0)\big|_{a_0=0} + b_1^2(y_{av,0}, a_0)\big|_{a_0=0} \\ &y_{av,0} = f_0(y_{av,0}, a_0)\big|_{a_0=0} \end{aligned} \tag{40}$$

and finds the required starting parameter together with the resulting average shift. For example, at $A_{ext} = 3\ m/s^2$, $W_0^{max} = 17.4\ nJ$, which corresponds to the point in fig. 6 where the envelope disappears (this A_{ext} corresponds to the lines 1a and 1b).

Now let us illustrate the presence of the boundary parameters required for oscillations in simulations of the behavioral VHDL-AMS model. Figure 8a shows a slowly growing ramp of acceleration (in ms^{-2}) as a function of the normalised time τ. At this A_{ext}, the displacement y is obtained as a function of time, fig. 8b. Below the boundary value of A_{ext}^{min}, the dynamics of the system are irregular with many local maxima detected in one period of oscillations (fig. 8c). As soon as the threshold of A_{ext} is passed, the oscillations are harmonic with one maximum detected during one period of oscillations (fig. 8d).

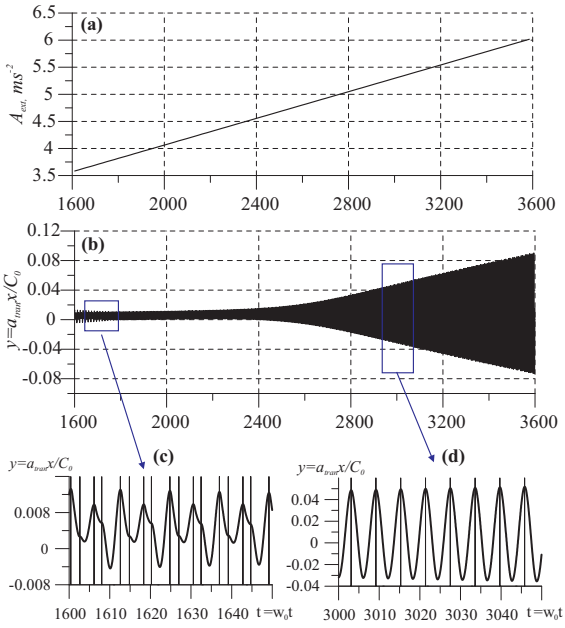

Fig. 8. Area overlap transducer: (a) slowly growing ramp of A_{ext} (the envelope of the external oscillations) and (b) corresponding displacement of the harvester as functions of normalised time. Two magnified waveforms show the case when no regular oscillations are observed (c) and when harmonic oscillations have started (d).

VI. Discussion and Conclusions

In this section we give a discussion of our theoretical approach, highlight the difference with the analytical tool from [14] and point out the immediate practical value of the results for design of e-VEHs.

The MSM is known as a powerful and flexible method for analysis of nonlinear systems. The two main practical benefits that we obtained from the theory are

- It allowed us to obtain equations that fully describe the oscillations in the system. Now, for any set of parameters, one can calculate the resulting oscillation and therefore converted power. It also gives the initial analysis of stability. The results obtained with this method have been used for further stability analysis in [25], [26]. Therefore, for the gap-closing transducer, based on the results presented in this paper, we define all possible dynamics of the system and find values of the system parameters where the system displays regular harmonic oscillations. Practically, this is very important since the conditioning circuit can operate correctly and effectively only if this is the case.
- Another conclusion that immediately follows from the method is the existence of 'boundary' values for the acceleration amplitude A_{ext} and the energy W_0 required to start oscillations in the resonator. The method yields a simple way to calculate these boundary values. This is also an important result from a practical standpoint: knowing parameters of the environment, one can optimize the design parameter W_0. For the area overlap transducer, the expressions that give the boundary values for A_{ext} and W_0 are very simple.

In addition, the method allows one to expand it to the case of different nonlinearities. This will allow the exploration of nonlinear effects that seem to be very promising for widening the frequency response of the system [27]–[29].

The limitations of the method follow from limitations that are inherit in perturbation techniques. Firstly, there is a very general condition for all perturbation methods that nonlinearities should be relatively small (this 'smallness' can be easily established in the normalised dimensionless equation by comparing the parameters of the nonlinear terms with unity). In our case, this is equivalent to stating that that the method will work while oscillations can be described as quasi-harmonic. As is shown by the simulations based on the VHDL-AMS model, this is typically the case for the system over a wide range of parameters. Secondly, despite the flexibility of the MSM, it demands that nonlinear terms should be arranged accurately with respect to the order of the small parameter ε. We note that for the gap-closing transducer we have overcome this difficulty by introducing a modification of the standard MSM implementation where we compensate an error that appeared due to the large constant shift $y_{av,0}$.

We also point out that all analytical results are verified by simulations of a realistic behavioral model carried out with VHDL-AMS/Eldo simulators.

References

[1] S. Roundy, P. Wright, and K. Pister, "Micro-electrostatic vibration-to-electricity converters," *Proceedings of 2002 ASME International Mechanical Engineering Congress*, novermber 2002.

[2] G. Despesse, T. Jager, J.J.Chaillout, J. M. Lger, A. Vassilev, S. Basrour, and B. Charlot, "Fabrication and characterization of high damping electrostatic micro devices for vibration energy scavenging," in *Proceeding of DTIP of MEMS & MOEMS conference*, 2005.

[3] P. Basset, D. Galayko, A. Paracha, F. M. A. Dudka, and T. Bourouina, "A batch-fabricated and electret-free silicon electrostatic vibration energy harvester," *Journal of Micromechanics and Microengineering*, vol. 19, no. 11, p. 115025, november 2009.

[4] S. Meninger, J. Mur-Miranda, R. Amirtharajah, A. Chandrakasan, and J. Lang, "Vibration-to-electric energy conversion," *Very Large Scale Integration (VLSI) Systems, IEEE Transactions on*, vol. 9, no. 1, pp. 64–76, 2001.

[5] B. C. Yen and J. H. Lang, "A variable-capacitance vibration-to-electric energy harvester," *IEEE Trans. Circuits Syst. I*, vol. 53, pp. 288–295, 2006.

[6] E. Torres and G. Rincón-Mora, "Electrostatic energy-harvesting and battery-charging cmos system prototype," *Circuits and Systems I: Regular Papers, IEEE Transactions on*, vol. 56, no. 9, pp. 1938–1948, 2009.

[7] M. Kiziroglou, C. He, and E. Yeatman, "Flexible substrate electrostatic energy harvester," *Electronics letters*, vol. 46, no. 2, pp. 166–167, 2010.

[8] E. O. Torres and G. A. Rincón-Mora, "Electrostatic energy-harvesting and battery-charging cmos system prototype," *IEEE transaction on circuits and systems - I: Regular Papers*, vol. 56, no. 9, pp. 1938–1948, september 2009.

[9] Y. Naruse, N. Matsubara, K. Mabuchi, M. Izumi, and S. Suzuki, "Electrostatic micro power generation from low-frequency vibration such as human motion," *Journal of Micromechanics and Microengineering*, vol. 19, p. 094002, 2009.

[10] D. Hoffmann, B. Folkmer, and Y. Manoli, "Fabrication, characterization and modelling of electrostatic micro-generators," *Journal of Micromechanics and Microengineering*, vol. 19, p. 094001, 2009.

[11] W. Ma, R. Zhu, L. Rufer, Y. Zohar, and M. Wong, "An integrated floating-electrode electric microgenerator," *Microelectromechanical Systems, Journal of*, vol. 16, no. 1, pp. 29–37, 2007.

[12] P. Mitcheson, E. Yeatman, G. Rao, A. Holmes, and T. Green, "Energy harvesting from human and machine motion for wireless electronic devices," *Proceedings of the IEEE*, vol. 96, no. 9, pp. 1457–1486, 2008.

[13] R. Guillemet, P. Basset, D. Galayko, and T. Bourouina, "Design optimization of an out-of-plane gap-closing electrostatic vibration energy harvester (veh) with a limitation on the output voltage," *Analog Integrated Circuits and Signal Processing*, pp. 1–9, 2011.

[14] D. Galayko and P. Basset, "A general analytical tool for the design of vibration energy harvesters (VEHs) based on the mechanical impedance concept," *IEEE Trans. Circuits Syst. I*, no. 99, pp. 299–311, 2011.

[15] B. Stark, P. Mitcheson, P. Miao, T. Green, E. Yeatman, and A. Holmes, "Converter circuit design, semiconductor device selection and analysis of parasitics for micropower electrostatic generators," *Power Electronics, IEEE Transactions on*, vol. 21, no. 1, pp. 27–37, 2006.

[16] A. Paracha, P. Basset, D. Galayko, F. Marty, and T. Bourouina, "A silicon MEMS dc/dc converter for autonomous vibration-to-electrical-energy scavenger," *Electron Device Letters, IEEE*, vol. 30, no. 5, pp. 481–483, 2009.

[17] P. Miao, P. Mitcheson, A. Holmes, E. Yeatman, T. Green, and B. Stark, "MEMS inertial power generators for biomedical applications," *Microsystem Technologies*, vol. 12, no. 10, pp. 1079–1083, 2006.

[18] D. Galayko, R. Guillemet, A. Dudka, and P. Basset, "Comprehensive dynamic and stability analysis of electrostatic vibration energy harvester (E-VEH)," in *2011 International Conference on Solid-State Sensors, Actuators and Microsystems (TRANSDUCERS)*, 2011, pp. 2382–2385.

[19] J. Miranda, "Electrostatic vibration-to-electric energy conversion," Ph.D. dissertation, Massachusetts Institute of Technology, Cambridge, MA, Feb. 2003.

[20] W. Tang, T. Nguyen, M. Judy, and R. Howe, "Electrostatic-comb drive of lateral polysilicon resonators," *Sensors and Actuators A: Physical*, vol. 21, no. 1-3, pp. 328–331, 1990.

[21] F. Pêcheux, C. Lallement, and A. Vachoux, "Vhdl-ams and verilog-ams as alternative hardware description languages for efficient modeling of multidiscipline systems," *Computer-Aided Design of Integrated Circuits and Systems, IEEE Transactions on*, vol. 24, no. 2, pp. 204–225, 2005.

[22] A. Nayfeh, *Introduction to perturbation techniques*. Wiley, 1993.

[23] A. Buonomo and A. Lo Schiavo, "On the theory of quadrature oscillations obtained through parallel LC VCOs," *IEEE Trans. Circuits Syst. I*, vol. 57, pp. 2509–2519, 2010.

[24] M. A. Karami and D. J. Inman, "Equivalent damping and frequency change for linear and nonlinear hybrid vibrational energy harvesting systems," *Journal of Sound and Vibration*, vol. 330, pp. 5583–5597, 2011.

[25] E. Blokhina, D. Galayko, R. Wade, P. Basset, and O. Feely, "Bifurcations and chaos in electrostatic vibration energy harvesters," in *IEEE International Symposium on Circuits and Systems 2012, Seoul, Korea, 20 – 24 May 2012*, 2012, pp. 397–400.

[26] E. O'Riordan, P. Harte, E. Blokhina, D. Galayko, and O. Feely, "Bifurcation scenarios in electrostatic vibration energy harvesters," in *proc. of the 2012 International Conference on Nonlinear Dynamics of Electronic Systems*, 11–13 July 2012, Wolfenbttel, Germany (accepted), 2012.

[27] F. Cottone, L. Gammaitoni, and H. Vocca, "Nonlinear energy harvesting," *Phys. Rev. Lett.*, vol. 102, p. 08061, 2009.

[28] S. Stanton, C. McGehee, and B. Mann, "Nonlinear dynamics for broadband energy harvesting: Investigation of a bistable piezoelectric inertial generator," *Physica D: Nonlinear Phenomena*, vol. 239, no. 10, pp. 640–653, 2010.

[29] L. Blystad, E. Halvorsen, and S. Husa, "Piezoelectric MEMS energy harvesting systems driven by harmonic and random vibrations," *Ultrasonics, Ferroelectrics and Frequency Control, IEEE Transactions on*, vol. 57, no. 4, pp. 908–919, 2010.